Available online at www.sciencedirect.com
ScienceDirect
Journal of Solid State Chemistry 181 (2008) 623–627
JOURNAL OF SOLID STATE CHEMISTRY
www.elsevier.com/locate/jssc

Synthesis, structure, magnetic properties and structural distortion under high pressure of a new osmate, Sr_2CuOsO_6

Michael W. Lufaso[a,*], William R. Gemmill[b], Samuel J. Mugavero III[b], Seung-Joo Kim[c], Yongjae Lee[d], Thomas Vogt[b], Hans-Conrad zur Loye[b]

[a]Department of Chemistry and Physics, University of North Florida, Jacksonville, FL 32224, USA
[b]Department of Chemistry and Biochemistry, University of South Carolina, Columbia, SC 29208, USA
[c]Department of Chemistry, Division of Energy Systems Research, Ajou University, Suwon 443-749, South Korea
[d]Department of Earth System Sciences, Yonsei University, Seoul 120-749, South Korea

Received 24 August 2007; received in revised form 18 December 2007; accepted 22 December 2007
Available online 31 December 2007

Abstract

A new osmate Sr_2CuOsO_6 was synthesized and its structure refined using powder synchrotron X-ray diffraction. The results of the Reitveld refinements indicate complete B-cation order in a double perovskite crystal structure. Furthermore, the analysis of the B-cation bond lengths indicates a symmetric coordination around Os, as opposed to a significant distortion of Cu–O bond lengths. The octahedral distortion around Cu(II) is characteristic of a Jahn-Teller distortion. Within the crystal structure of Sr_2CuOsO_6, the long Cu–O bonds are aligned in the same direction along the *c*-axis in the tetragonal unit cell. This parallel arrangement of long Cu–O bonds produces a lattice parameter ratio, $c/(2^{1/2}a)$, that is greater than unity. The magnetic susceptibility of Sr_2CuOsO_6 was measured using a SQUID magnetometer and was observed to be consistent with an assignment of Cu(II)–Os(VI) formal oxidation states, thus confirming the bond valences calculated on the basis of the crystal structure. In perovskites, octahedral tilting and bond shortening are two competing compression mechanisms. Compression mechanisms of this double perovskite were characterized using high-pressure synchrotron X-ray diffraction. Application of hydrostatic pressure up to 6 GPa significantly decreased the lattice parameter ratio, demonstrating the primary compression mechanism is a shortening of the long Cu–O bond.

Keywords: Perovskite; High pressure; Compression mechanism; Jahn-Teller

1. Introduction

The perovskite structure (ABX_3) has a large number of reported compounds and the variety of physical properties of perovskites has sustained interest in these materials. Substitutions on the octahedral *B*-site may lead to a double perovskite with a cation order for $AB_{1/2}B'_{1/2}O_3$ when the charge and/or size of B and B′ are suitably different. Cation ordering leads to the structure type commonly referred to as a double perovskite, which may also undergo octahedral tilting distortions depending on the relative sizes of the A- and B-cation. Compounds containing osmium with a structure related to a perovskite include Ba_2MOsO_6 (M = Li, Na) [1], Sr_2MOsO_6 (M = Li, Na, Mg, Ca, Fe, Co, Sc, Cr, In, and Ga) [2], Sr_2CrOsO_6 [3], A_2NiOsO_6 (A = Ca, Sr) [4], Ln_2NaOsO_6 (Ln = La, Pr, Nd) [5], and Ln_2LiOsO_6 (Ln = La, Pr, Nd, Sm) [6]. The double perovskite Sr_2CrOsO_6 has interesting magnetic properties and has been reported to have a very high Curie temperature (~725 K). Osmium-containing oxides are relatively rare because of safety concerns and difficulties in the synthesis which are both related to the relatively high volatility of OsO_4. In this study, we have used a sealed quartz tube under static vacuum to minimize the loss of osmium during synthesis.

Perovskites are known to undergo structural distortions induced by changes in temperature and pressure; recent examples include a pressure-induced structural phase transition to a lower symmetry perovskites in Ba_2BiTaO_6

*Corresponding author. Fax: +1 904 620 1989.
E-mail address: michael.lufaso@unf.edu (M.W. Lufaso).

0022-4596/$ - see front matter © 2007 Elsevier Inc. All rights reserved.
doi:10.1016/j.jssc.2007.12.021

and Ba_2YTaO_6 [7,8]. In many perovskites, the 12-coordinate *A*-site is more compressible than the 6-coordinate *B*-site and application of high pressure results in a lowering of the effective tolerance factor. In the majority of reported crystal structures of perovskites containing Jahn-Teller distortions, the manganates typically have alternating distortions of the long Mn–O bonds whereas cuprates tend to have long Cu–O bonds aligned in the same direction [9]. There are exceptions to this general observation including the long Mn–O aligned in Sr_2MnSbO_6 and alternating long Cu–O bonds in $SrLaCuSbO_6$ [10,11]. High-pressure X-ray diffraction studies were undertaken to determine the effect of pressure upon the structure and octahedral tilting of Sr_2CuOsO_6 and the type of compression mechanism that is dominant. In the present paper, we report the synthesis, crystal structure, magnetic properties, and high-pressure X-ray diffraction studies of a new osmate, Sr_2CuOsO_6.

2. Experimental

2.1. Synthesis

A polycrystalline sample of Sr_2CuOsO_6 was prepared by mixing a 2:1:1 molar ratio of SrO:CuO:Os, SrO prepared by heating $Sr(OH)_2 \cdot H_2O$ (Alfa, 99.9%) in air at 1000 °C for 12 h, CuO (Alfa, 99.99%), and Os powder (J & J Materials, Inc., 99.98%), in an agate mortar and pestle inside a glovebox. The reaction mixture was transferred to an alumina crucible and placed in a quartz ampoule. A slight excess of the stoichiometric amount of Ag_2O needed to oxidize the Os was added to a separate alumina crucible. The reaction ampoule containing the two crucibles was sealed under high vacuum. The reaction mixture was heated in a vertical tube furnace at a rate of 10 °C/min to 800 °C, held at temperature for 24 h, and then cooled to room temperature by turning off the furnace. The reaction mixture was heated in a glass ampoule under high vacuum for a second and third time at 825 °C for periods of 24 h without the presence of any Ag_2O in the reaction vessel. Phase purity was established using X-ray powder diffraction data collected using a Rigaku DMAX 2200 diffractometer. The sample had small amount of $SrCO_3$ as a secondary phase.

2.2. Synchrotron high- and ambient-pressure X-ray diffraction

Ambient temperature and high-pressure powder X-ray diffraction data were collected at the X7A beam-line at the National Synchrotron Light Source at Brookhaven National Laboratory. At ambient pressure, the samples was mounted in a thin capillary tube and spun during data collection to minimize preferred orientation. A wavelength of 0.690413 Å was selected and data were collected using a position-sensitive detector (PSD) over the range 7–60° 2θ. *In situ* high-pressure synchrotron X-ray powder diffraction experiments on Sr_2CuOsO_6 were performed using a diamond anvil cell (DAC). The primary white beam from the bending magnet was monochromated and focused using an asymmetrically cut bent Si(1 1 1) crystal. A tungsten wire crosshair was positioned at the center of the goniometer circle and subsequently the position of the incident beam was adjusted to the crosshair. A gas proportional PSD was stepped in 0.25° intervals over the angular range of 5–35° in 2θ with counting times of 60–75 s per step. The wavelength of the incident beam (0.64824(4) Å), PSD zero channel and PSD degrees/channel were determined from a CeO_2 standard (SRM 674). The polycrystalline samples were loaded into the DAC at ambient pressure and room temperature along with a few small ruby spheres. The DAC is based on a modified Merrill-Bassett design and employs two diamonds with 0.5 mm diameter culets on tungsten-carbide supports. The X-rays are admitted by a 0.5 mm diameter circular aperture, and the exit beam leaves via a 0.5×3.0 mm rectangular tapered slit, oriented perpendicular to the horizontal plane of the diffractometer. The sample chamber is composed of a ~100 μm diameter hole made using a spark-erosion method in the center of a 250 μm thick stainless-steel gasket, pre-indented to 150 μm thickness before erosion. The DAC was placed on the second axis of the diffractometer, and the sample position was adjusted using a pre-centered microscope. The pressure at the sample was measured by detecting the shift in the R1 emission line of the included ruby. No evidence of nonhydrostatic conditions or pressure anisotropy were detected during our experiments, and the R1 peaks from three included ruby chips remained strong and sharp with deviations in the measured pressure of less than 0.15 GPa. A methanol–ethanol–water mixture with component ratio of 16:3:1 was used as a pressure medium. Refinements of data collected at different applied pressures were performed using EXPGUI GSAS [12,13]. A pseudo-Voigt function was used to model the peak profile and the background was described by interpolation of selected points. The angular range employed in the refinements was from 6° to 35° 2θ and excluded the regions which contained strong Bragg peaks from the pressure cell gasket.

2.3. Magnetic measurements

Magnetic susceptibility measurements were performed on Sr_2CuOsO_6 using a Quantum Design MPMS XL SQUID magnetometer. The sample was measured under both zero field cooled (ZFC) and field cooled (FC) conditions in applied fields of 1 and 10 kG over the temperature range of $2\,K < T < 300\,K$. The sample was contained in a gel capsule suspended in a plastic straw for immersion into the SQUID. The small diamagnetic contribution of the gelatin capsule containing the sample had negligible contribution to the overall magnetization, which was dominated by the sample.

3. Results and discussion

3.1. Crystal structure

The target compound Sr_2CuOsO_6 was synthesized as a well-crystallized powder with a small detectable amount of a secondary phase $SrCO_3$, which is presumed to have formed when unreacted SrO reacted with atmospheric CO_2. The laboratory diffraction pattern could be indexed with a tetragonal unit cell with $a \approx 5.39$ Å and $c \approx 8.49$ Å. The structure was quickly established as a double perovskite and the systematic absences were consistent with space groups $I4/mmm$, $I4mm$, and $I4/m$. Starting structure models for use in the Rietveld refinements were obtained from the literature [10,14]. The best refinement was obtained using the structure model with space group $I4/m$. The background was fitted using a linear interpolation function with manually selected points. The isotropic thermal parameter for O(1) and O(2) was constrained to be equal. Attempts were made to refine the cation ordering of the Cu and Os, which indicated complete ordering within the limits of the technique and were fixed. Complete ordering of the *B*-site cations is consistent with the large difference in charge and size between the Cu^{2+} and Os^{6+}. Observed and calculated X-ray diffraction pattern for Sr_2CuOsO_6 is shown in Fig. 1 and the crystallographic data and atomic coordinates are given in Table 1. Final fit statistics were $R_{wp} = 4.72\%$, $R_p = 3.53\%$, $R(F^2) = 7.61\%$.

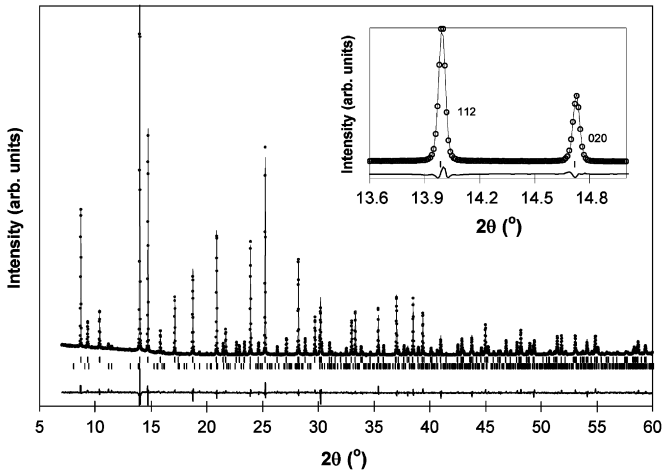

Fig. 1. Observed and calculated X-ray diffraction pattern for Sr_2CuOsO_6. The difference between observed and calculated intensities is shown at the bottom. Tick marks indicate allowed Bragg reflections for Sr_2CuOsO_6 (top) and $SrCO_3$ (bottom). The inset shows the splitting of the (112 and 020) reflections near 14° 2θ, which is indicative of tetragonal symmetry in ordered-double perovskites.

Selected interatomic distances and bond angles from the refined crystal structure are given in Table 2. Bond valence sums for Sr and Cu are 2.13 and 2.07 v.u., respectively. The R_o parameter for the relatively rarely reported Os^{6+} is 2.03 [15], which suggests a 2.03 Å Os–O bond length for six coordinate Os, whereas Shannon [16] indicates a 1.90 Å Os–O bond length. Two typical Os(VI)–O bond lengths in perovskites are 1.91 and 1.92 Å for Sr_2NiOsO_6 and Ca_2NiOsO_6, respectively, and are in good agreement with the lengths in this study [4]. Both an octahedral tilting distortion and a distortion of the octahedral bond lengths are two types of distortions from the ideal aristotype perovskite in the crystal structure of Sr_2CuOsO_6. The Cu–O bond distances indicate a significant lengthening of the Cu–O(1) bonds at 2.315(6) Å versus 1.994(5) Å for the O(2) bonds, indicative of the presence of a Jahn-Teller distortions. The Jahn-Teller distortions are aligned parallel to the *c*-axis. Octahedral tilting, approximately 11°, occurs by rotation about the *c*-axis in an out-of-phase arrangement. The crystal structure of Sr_2CuOsO_6 given in Fig. 2 illustrates the presence of both out-of-phase octahedral tilting and elongation distortions.

Table 2
Selected interatomic distances (Å) and bond angles (°) for Sr_2CuOsO_6 at ambient pressure

Atom–atom	Distance (Å)
Sr–O(1)	2.7018(4) (× 4)
Sr–O(2)	2.621(3) (× 4)
Sr–O(2)	3.110(4) (× 4)
Cu–O(1)	2.315(6) (× 2)
Cu–O(2)	1.994(5) (× 4)
Os–O(1)	1.928(6) (× 2)
Os–O(2)	1.888(5) (× 4)
Atom–atom–atom	Angle (°)
Cu–O(2)–Os	158.1(3)

Table 1
Crystallographic data and atomic coordinates for Sr_2CuOsO_6 at ambient pressure

Space group volume	$I4/m$ 246.5329(14) Å^3	Lattice parameters		$a = 5.38985(1)$ Å $c = 8.48635(4)$ Å
Atom	*x*	*y*	*z*	$U_i/U_e \times 100$ (Å^2)
Sr	0	$\frac{1}{2}$	$\frac{1}{4}$	1.42(3)
Cu	0	0	0	0.67(4)
Os	$\frac{1}{2}$	$\frac{1}{2}$	0	0.68(1)
O(1)	0	0	0.2728(7)	1.19(11)
O(2)	0.3054(9)	0.2088(9)	0	1.19(11)

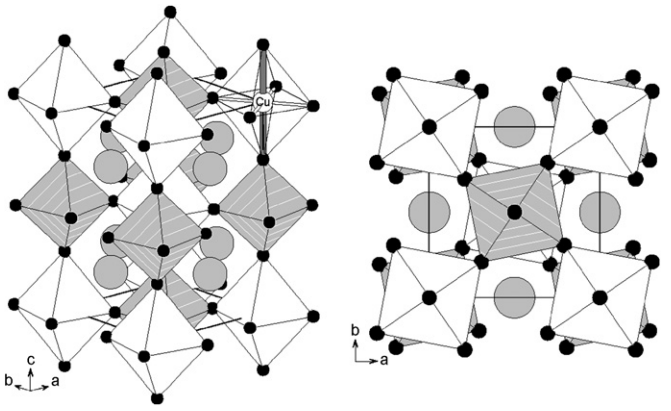

Fig. 2. Crystal structure of Sr_2CuOsO_6. Copper is located in the center of the white octahedra, Os are inside the gray octahedra, gray spheres represent Sr, and black spheres represent oxygen. Jahn-Teller distortions are parallel to the c-axis and the long Cu–O bond is shown in think gray. Octahedral tilting occurs by rotation about the c-axis in an out of phase arrangement with a tilt angle of approximately 11°.

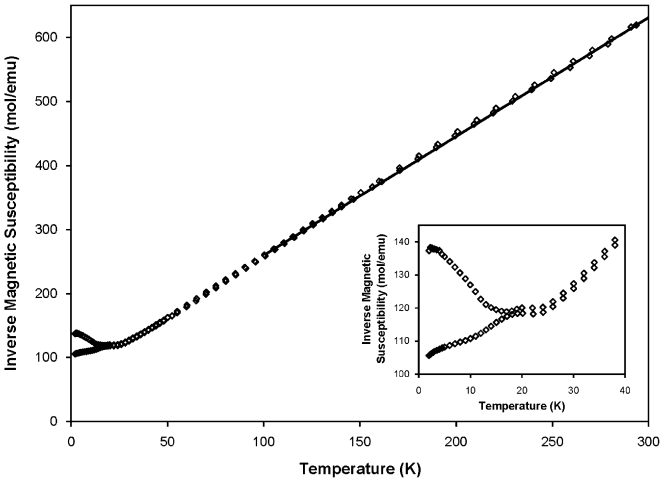

Fig. 3. Temperature dependence of the inverse magnetic susceptibility in an applied field of 10 kG. Zero field cooled (ZFC) data are triangles and field cooled (FC) data are circles. A fit to the Curie–Weiss law gave $\mu_{eff} = 2.07\,\mu_B$, $C = 1.86$ emu/(K mol) and $\theta = -40$ K.

3.2. Magnetism

The temperature dependence of the magnetization for Sr_2CuOsO_6 in an applied field of 10 kG is shown in Fig. 3. Fitting the high-temperature susceptibility ($100 < T < 300$) to the Curie–Weiss law, given by $X_{CW} = C/(T-\theta)$ where C is the Curie constant, and θ is the Curie–Weiss temperature, results in values of $\mu_{eff} = 2.07\,\mu_B$, $C = 1.86$ emu/(K mol), and $\theta = -40$ K. The theoretical spin-only value for d^2 Os(VI) and d^9 Cu(II) cation is $2.35\,\mu_B$, the experimental value is slightly lower than expected for Os(VI) due to the presence of spin–orbit coupling [17]. At low temperatures, an upturn in the magnetization is evident. The negative Weiss constant (−40 K) and the plot of the magnetization as a function of temperature, which shows a sudden upturn at about 18 K, is indicative of antiferromagnetic correlations. The ZFC and FC data do not overlay below ~20 K and is indicative of antiferromagnet with sufficiently small domains or formation of a spin glass.

Table 3
Pressure dependence of the unit cell volume and lattice parameters of Sr_2CuOsO_6 at a pressure up to 5.62 GPa

Pressure (GPa)	a (Å)	c (Å)	Volume (Å^3)
0.26	5.4020(2)	8.4669(5)	247.07(2)
0.68	5.3942(2)	8.4462(4)	245.77(2)
1.61	5.3809(1)	8.4119(3)	243.56(1)
2.70	5.3757(5)	8.3983(15)	242.70(5)
4.42	5.3630(3)	8.3754(10)	240.89(4)
5.62	5.3607(4)	8.3691(10)	240.50(4)

The uncertainty in the measured pressure is 0.15 Gpa.

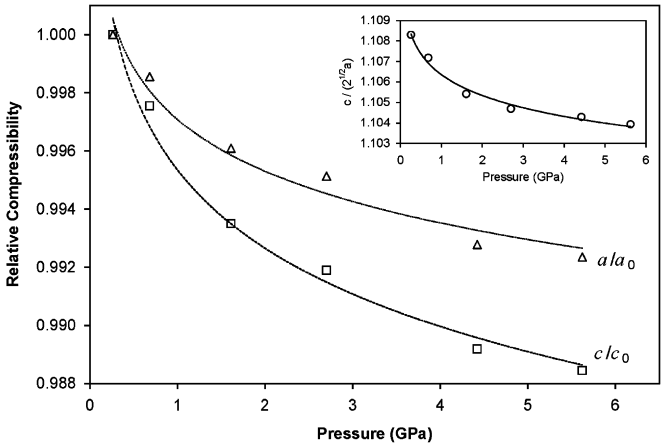

Fig. 4. Relative compressibility of lattice parameters. The c lattice parameter is much more compressible than the a because of the high compressibility of the Jahn-Teller distorted Cu–O bonds. Triangles represent a/a_0 and squares represent c/c_0, where a_0 and c_0 represent refined lattice parameters of data collected at 0.26 GPa. The inset shows the pressure dependence of the lattice parameter ratio, $c/2^{1/2}a$. The decrease in the lattice parameter ratio indicates bond compression along the c-axis is preferred over changes in the magnitude of the octahedral tilting angle. Uncertainties in the ratio are smaller than the symbol size. The lines are a guide to the eye.

3.3. High-pressure X-ray diffraction

The pressure dependence of the lattice parameters and unit cell volume is given in Table 3. The relative compressibility of the lattice parameters is given in Fig. 4 and the pressure dependence of the lattice parameter ratio $c/(2^{1/2}a)$ is shown in the inset. The trends indicate a higher relative compressibility of the c lattice parameter compared to the a lattice parameter. The long Cu–O bonds aligned along the c-axis are more compressible than those along the a-axis. A similar high compressibility along the c-axis was also observed for A_2CuWO_6 (A = Sr, Ba) [18]. Even at the highest applied pressure, there were no changes evident in the diffraction peaks to indicate a pressure-induced phase transition. The bulk modulus was obtained by fitting a second-order

Birch–Murnaghan equation of state to the pressure dependence data up to 5.6 GPa. The bulk modulus is 229(25) GPa in the limited pressure range of this study. The bulk modulus is slightly larger than the isostructural ordered-double perovskite Sr_2CuWO_6, which was 185(14) GPa [18].

In conclusion, a new Cu(II)–Os(VI) containing ordered-double perovskite has been synthesized and characterized using ambient and high-pressure synchrotron X-ray powder diffraction and magnetic measurements. The Jahn-Teller distortion results in long Cu–O bonds aligned in the same direction along the *c*-axis in the tetragonal unit cell. Application of hydrostatic pressure up to 6 GPa significantly decreased the lattice parameter ratio, $c/(2^{1/2}a)$, and when taken with the relative compressibilities of the *a* and *c* axes, demonstrates the primary compression mechanism in Sr_2CuOsO_6 is a shortening of the long Cu–O bond. The results of this study indicate the opportunity for additional investigations, conducted at greater applied pressures, in order to determine if there exists a changeover in the primary compression mechanism from shortening of the long Cu–O bond to changes in octahedral tilting.

References

[1] K.E. Stitzer, M.D. Smith, H.-C. zur Loye, Solid State Sci. 4 (2002) 311.
[2] A.W. Sleight, J. Longo, R. Ward, Inorg. Chem. 1 (1962) 245.
[3] Y. Krockenberger, K. Mogare, M. Reehuis, et al., Phys. Rev. B 75 (2007) 020404/1.
[4] R. Macquart, S.-J. Kim, W.R. Gemmill, J.K. Stalick, Y. Lee, T. Vogt, H.-C. zur Loye, Inorg. Chem. 44 (2005) 9676.
[5] W.R. Gemmill, M.D. Smith, R. Prozorov, H.-C. zur Loye, Inorg. Chem. 44 (2005) 2639.
[6] W.R. Gemmill, M.D. Smith, H.-C. zur Loye, J. Solid State Chem. 179 (2006) 1750.
[7] K.S. Wallwork, B.J. Kennedy, Q.D. Zhou, Y. Lee, T. Vogt, J. Solid State Chem. 178 (2005) 207.
[8] M.W. Lufaso, R. Macquart, Y. Lee, T. Vogt, H.-C. zur Loye, Chem. Commun. (2006) 168.
[9] M.W. Lufaso, P.M. Woodward, Acta Cryst. B 60 (2004) 10.
[10] M.W. Lufaso, P.M. Woodward, J. Goldberger, J. Solid State Chem. 177 (2004) 1651–1659 and references therein.
[11] M.P. Attfield, P.D. Battle, S.K. Bollen, S.-H. Kim, A.V. Powell, M. Workman, J. Solid State Chem. 96 (1992) 344–359.
[12] A.C. Larson, R.B. von Dreele, General Structure Analysis System (GSAS), Los Alamos National Laboratories, 1990.
[13] B.H. Toby, J. Appl. Crystallogr. 34 (2001) 210.
[14] M. Gateshki, J.M. Igartua, E. Hernandez-Bocanegra, J. Phys.: Condens. Matter 15 (2003) 6199.
[15] I.D. Brown, D. Altermatt, Acta Cryst. B B41 (1985) 244.
[16] R.D. Shannon, Acta Cryst. A 32 (1976) 751.
[17] J.R. Plaisier, R.J. Drost, D.J.W. IJdo, J. Solid State Chem. 169 (2002) 189.
[18] M.W. Lufaso, W.R. Gemmill, S.J. Mugavero, Y. Lee, T. Vogt, H.-C. zur Loye, J. Solid State Chem. 179 (2006) 3556.